CHEMISTRY OF MATERIALS

Article

pubs.acs.org/cm

Magnetism in Ca_2CoOsO_6 and Ca_2NiOsO_6: Unraveling the Mystery of Superexchange Interactions between 3d and 5d Ions

Ryan Morrow,[†] Kartik Samanta,[‡] Tanusri Saha Dasgupta,*[,‡] Jie Xiong,[†] John W. Freeland,[§] Daniel Haskel,[§] and Patrick M. Woodward*[,†]

[†]Department of Chemistry and Biochemistry, The Ohio State University, Columbus, Ohio 43210-1185, United States

[‡]Department of Condensed Matter Physics and Materials Sciences, S. N. Bose National Centre for Basic Sciences, JD Block, Sector III, Salt Late, Kolkata 700098, India

[§]Advanced Photon Source, Argonne National Laboratory, 9700 Cass Avenue, Argonne, Illinois 60439, United States

Supporting Information

ABSTRACT: In order to rationalize and predict the behavior of compounds containing 5d transition metal ions, an understanding of the local moments and superexchange interactions from which their magnetic properties are derived is necessary. The magnetic and electrical properties of the ferrimagnetic double perovskites Ca_2CoOsO_6 and Ca_2NiOsO_6 studied here provide critical insight toward that goal. First-principles density functional theory (DFT) calculations indicate, and experimental measurements confirm, that the Os(VI) moments are directed antiparallel to the Co/Ni moments. X-ray magnetic circular dichroism (XMCD) measurements reveal that the orbital moment on osmium has a magnitude that is approximately 30% of the spin moment, and the two contributions oppose each other. Both the size and direction of the orbital moment are confirmed by the DFT calculations. The size of the Os(VI) total moment is predicted to be 0.6−0.7 μ_B by DFT calculations. The ferrimagnetic ground state is stabilized by strong antiferromagnetic coupling between the d^2 Os(VI) ion and the d^8/d^7 Ni(II)/Co(II) ion. Not only does the observation of antiferromagnetic coupling violate the Goodenough−Kanamori rules, but also it is unusual in that it becomes stronger as the Os−O−Co/Ni bond angle decreases. This unusual behavior is shown to arise predominantly from coupling between Os t_{2g} orbitals and Ni/Co e_g orbitals, mediated by the intervening oxide ion. We further find that both compounds are spin−orbit assisted Mott insulators.

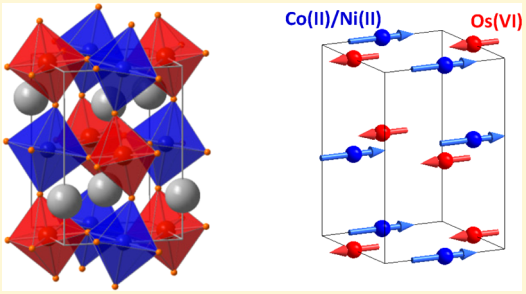

INTRODUCTION

The electrical and magnetic properties of oxides containing 5d elements differ from those containing 3d elements in some significant ways. The 5d orbitals hybridize more strongly with oxygen, which often leads to metallic conductivity and Pauli paramagnetism. Even in those compounds where the valence electrons are localized, differences in crystal-field splitting, the larger spatial extent of the 5d orbitals, and the presence of strong spin−orbit coupling (SOC) can lead to interesting and unexpected magnetic behavior. For example, the layered perovskite Sr_2IrO_4 is an insulator that orders antiferromagnetically at 240 K[1,2] while its isoelectronic 4d counterpart Sr_2RhO_4 is metallic and does not show long-range magnetic order.[3] In a similar vein La_3OsO_7 and La_3RuO_7 are isoelectronic and isostructural, but adopt different antiferromagnetic structures.[4−6] Li_2IrO_3 and Na_2IrO_3, both of which possess layers with a honeycomb pattern of iridium atoms, are thought to be tantalizingly close to one of the most exotic and elusive types of magnetism, a spin liquid.[7−9] The excitement surrounding 5d oxides is further fueled by theoretical predictions of exotic states of matter, such as the Weyl semimetallic state, whose existence is predicted to arise from the combined effects of strong SOC and electron correlations.[10]

To understand the magnetism of the 5d oxides one must first understand the sign and strength of superexchange interactions between magnetic centers. Among 3d transition metal oxides the venerable Goodenough−Kanamori (G-K) rules are useful predictors of superexchange interactions in a qualitative sense.[11,12] However, the G-K rules often fail to predict even the sign of the superexchange coupling between 3d ions and 5d ions, where a mismatch in the energies of the d-orbitals complicates matters.

The magnetism of Sr_2FeOsO_6 and Ca_2FeOsO_6, both of which contain Os(V) and Fe(III), highlights the shortcomings of the G-K rules in mixed 3d−5d oxides. The combination of d^3 and high-spin d^5 ions is the textbook case for ferromagnetic superexchange coupling according to the G-K rules. In spite of this, Sr_2FeOsO_6 orders antiferromagnetically on cooling below 140 K, with a magnetic structure that contains antiferromag-

Received: January 19, 2016
Revised: May 13, 2016

DOI: 10.1021/acs.chemmater.6b00254
Chem. Mater. XXXX, XXX, XXX−XXX

netic nearest neighbor coupling in the *ab*-plane where the Os−O−Fe bonds are bent, and ferromagnetic coupling in the *c*-direction where the bonds are linear (i.e., the C-type AFM structure).[13,14] It is tempting to attribute the breakdown of the G-K rules to nonlinearity of the bonds in the *ab*-plane, but that line of reasoning fails to explain the magnetic structure that emerges when the sample is cooled below 65 K, which retains antiferromagnetic coupling in the *ab*-plane, but transforms to an up−up−down−down pattern of spins in the *c*-direction, despite the fact that the Os−O−Fe bonds in that direction remain linear.

In Ca_2FeOsO_6, where the smaller Ca^{2+} ion has replaced Sr^{2+}, additional tilting of the octahedra lowers the symmetry to monoclinic and results in Os−O−Fe bonds that are bent (151−153°) in all three directions. The magnetic ground state now becomes ferrimagnetic, and the magnetic ordering temperature more than doubles (T_C = 350 K).[14,15] A similar crossover from antiferromagnetism to ferrimagnetism is observed as the tolerance factor decreases for A_2CoOsO_6, A_2NiOsO_6, and A_2CuOsO_6 (A = Sr, Ca).[17−23] Application of hydrostatic pressure can also be used to transform Sr_2FeOsO_6 into a ferrimagnet but, interestingly, does not appear to trigger a structural transition from tetragonal to monoclinic symmetry.[15] The extreme sensitivity to chemical and external pressure highlights the delicate competition between various superexchange interactions in mixed 3d−5d oxides.[24]

In this paper we take a detailed look at the electronic structure, magnetic, and electrical properties of two ferrimagnetic double perovskites, Ca_2CoOsO_6 (T_C = 145 K) and Ca_2NiOsO_6, (T_C = 175 K).[20,21] Interestingly, neutron diffraction studies do not provide clear evidence for a detectable moment on osmium in either compound. Despite the fact that several Os(VI) double perovskites have been studied in the literature, such as Ba_2CaOsO_6, Ca_2CaOsO_6, and Sr_2MgOsO_6,[25−28] an Os(VI) moment has yet to be observed using neutron powder diffraction (NPD). Thompson et al. have attempted to observe the Os(VI) moment in Ba_2CaOsO_6 with NPD, but its ordered magnitude was below the detection limit of the instrument used in that study.[25] In the absence of SOC, a moment of 2 μ_B is expected for a d^2 ion like Os (VI) in the strong field limit that is applicable to the magnetically ordered state. A reduction of the moment due to SOC as well as covalency with oxygen is expected, but the sizes of these effects are not well-understood.

The ferrimagnetism of Ca_2CoOsO_6 and Ca_2NiOsO_6 allows the use of X-ray magnetic circular dichroism to directly probe the local spin and orbital moments on each transition metal ion. This direct spectroscopic probe is combined with electronic structure calculations and magnetometry to develop a comprehensive picture of the local magnetism and magnetic coupling in these two compounds. In addition, electrical transport properties are also measured. The experimental findings are further corroborated in terms of first-principles density functional theory (DFT) calculations. The results have important implications for the larger family of mixed 3d−5d oxides.

EXPERIMENTAL SECTION

Powder samples of approximately 1.5 g were prepared via the solid state method by grinding stoichiometric amounts of CaO (99.9% pure, Sigma-Aldrich), Co_3O_4 (99.8% pure, Fischer Scientific), or NiO (99.998%, Alfa Aesar), and Os metal (99.98% pure, Alfa Aesar), with a mortar and pestle in a glovebox. Next, the mixture was placed in a loosely capped alumina tube that was loaded into a silica tube (3 mm thick walls, approximate volume 40 mL) along with a secondary vessel containing PbO_2. The tubing was sealed under dynamic vacuum before being heated to 1000 °C for a period of 48 h. PbO_2 decomposes at these elevated temperatures serving as an *in situ* source of O_2 gas. A calculated excess of 0.25 mol O_2 per mole of product is used to ensure full oxidation of the reactants. The use of sealed reaction tubes and placement of the furnace within a fume hood are essential to avoid contact with the volatile and highly toxic OsO_4 gas. The reactions are described by the following equations:

$$12CaO + 2Co_3O_4 + 6Os + (19PbO_2) \rightarrow 6Ca_2CoOsO_6 + (19PbO) + 3/2O_2$$

$$4CaO + 2NiO + 2Os + (7PbO_2) \rightarrow 2Ca_2NiOsO_6 + (7PbO) + 1/2O_2$$

The field dependence of the magnetization of Ca_2CoOsO_6 and Ca_2NiOsO_6 powder was measured at 5 K between maximum fields of ±5 T using a Quantum Design Magnetic Property Measurement System (MPMS) SQUID magnetometer. Powders were also pressed into pellets, sintered overnight at 1000 °C in a sealed silica ampule, and cut into bar shapes for electrical conductivity measurements. Copper wire leads were attached to the pellets in a 4-point probe geometry with silver adhesive, allowing for conductivity measurements using a Quantum Design Physical Property Measurement System (PPMS). Measurements were conducted within the temperature range 30−400 K for Ca_2CoOsO_6 and 120−400 K for Ca_2NiOsO_6. The lower temperature limit was the point below which the sample became too resistive to accurately measure.

X-ray absorption spectroscopy (XAS) and X-ray magnetic circular dichroism (XMCD) data were collected at the L_2 and L_3 edges of the 3d transition metal ion on the 4-ID-C beamline at the Advanced Photon Source (APS) at a temperature of 10 K. Similar measurements were conducted on the 4-ID-D beamline at the APS to measure the higher energy 5d Os L edges at a temperature of 5 K. Each measurement was repeated in opposing magnetic fields of +3.5 and −3.5 T and combined in order to remove any artifacts of nonmagnetic origin. Each spectrum was normalized to the size of the step height, and a 2:1 ratio of the L_3 and L_2 edge steps was assumed. The energy scale of each 3d spectrum was aligned by the simultaneous collection of a standard reference.

COMPUTATIONAL DETAILS

The first-principles results described in the paper are obtained in full potential linear augmented plane wave (FLAPW) basis as implemented in the WIEN2k code.[29] For LAPW calculations, we chose the APW+lo as the basis set, and the expansion in spherical harmonics for the radial wave functions was taken up to l = 10. The charge densities and potentials were represented by spherical harmonics up to l = 6. The commonly used criterion for the convergence of basis set RMT*K_{max} was chosen to be 7.0, where K_{max} is the plane wave cutoff and RMT is the smallest atomic sphere radius.

The exchange correlation functional for the self-consistent calculations was chosen to be that of generalized gradient approximation (GGA).[30] To check the missing correlation energy at transition metal sites beyond GGA, calculations with supplemented Hubbard U (GGA+U)[31] were carried out, with choice of U (Co/Ni) = 4 eV, U (Os) = 2 eV, and Hund's coupling, J_H = 0.8 eV. Results have been cross-checked in terms of variation of U values over 1−2 eV. Spin−orbit coupling has been included in the calculations as the second variational form to the original Hamiltonian. Additionally, the muffin-tin orbital (MTO)-based linear muffin-tin orbital (LMTO)[32] method and the *N*th-order MTO method, namely, NMTO method[33] as implemented in the STUTTGART code were employed. The NMTO method, which relies on self-consistent potential generated by the LMTO method, has been used for deriving the low-energy Hamiltonian defined in the basis of effective Co/Ni-d and Os-d Wannier functions, by integrating out the degrees of freedom related

DOI: 10.1021/acs.chemmater.6b00254
Chem. Mater. XXXX, XXX, XXX−XXX

to Ca and O. The real-space representation of the low-energy Hamiltonian provides the information on crystal-field splitting at B (Co/Ni) and Os sites as well as effective hopping interactions between the two.

RESULTS

To properly interpret the magnetic behavior of these compounds it is necessary to first determine if they are localized electron insulators or itinerant electron conductors. The dc electrical conductivities of Ca_2CoOsO_6 and Ca_2NiOsO_6, as measured by the 4-point probe method on sintered polycrystalline pellets are shown in Figure 1a. Both

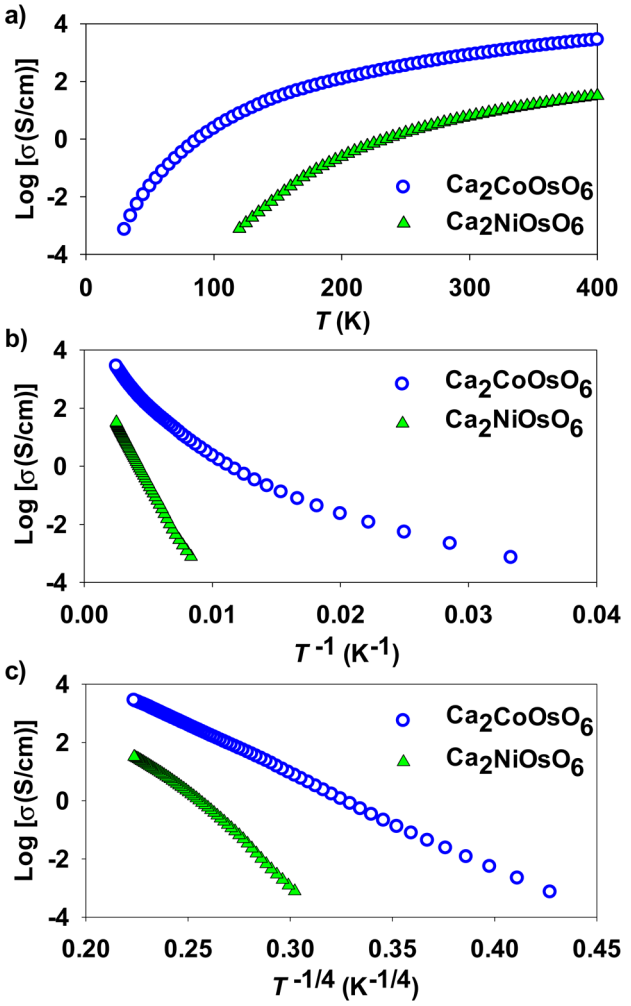

Figure 1. Temperature dependence of the electrical conductivity of Ca_2CoOsO_6 and Ca_2NiOsO_6 shown on (a) a linear temperature scale, (b) an inverse temperature scale, and (c) a $T^{-1/4}$ scale.

materials exhibit insulating behavior, with conductivities that decrease by several orders of magnitude as the temperature is lowered. Attempts were made to plot the data according to an activated transport model, Figure 1b, and a variable range hopping model, Figure 1c. The data for Ca_2NiOsO_6 are linear on a T^{-1} scale, with a slope corresponding to an estimated energy gap of 0.33 eV. Ca_2CoOsO_6, which is clearly nonlinear on a T^{-1} scale, is found to be linear on a $T^{-1/4}$ scale, in accordance with a three-dimensional variable range hopping transport model.[34] Similar behavior has been reported for other osmate double perovskites.[14,17,19] While it should be noted that the mechanism of conduction can be influenced by the polycrystalline nature of the pellets used for these measurements, both materials are clearly insulating.

To understand the insulating behavior of these two compounds we next turn to electronic structure calculations. The electronic densities of states (DOS) for Ca_2CoOsO_6 obtained from GGA+U+SOC calculations are shown in Figure 2. The contributions from both transition metals and oxygen

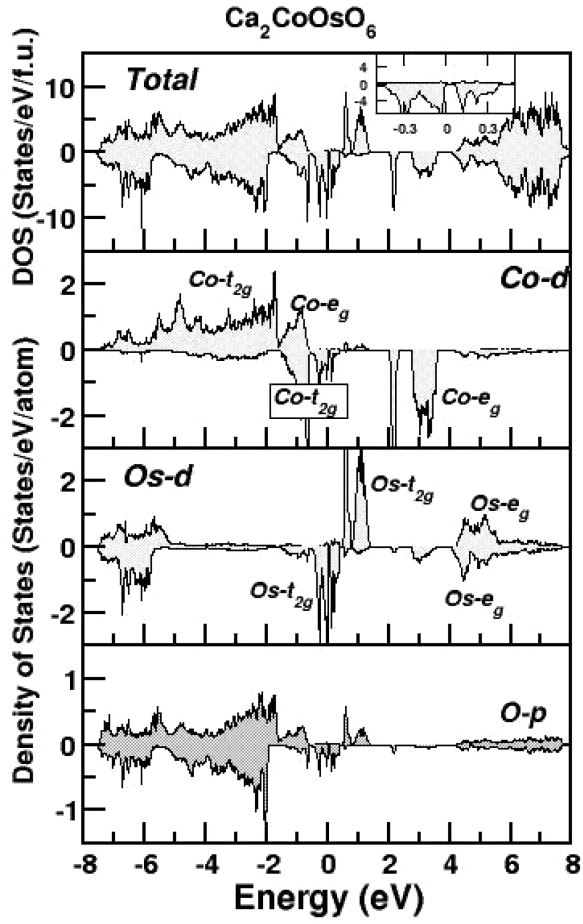

Figure 2. Spin dependent partial density of states plots for Ca_2CoOsO_6 as given by GGA+U+SOC calculations. The Fermi level is set to zero energy. The inset in the upper panel highlights the region near the Fermi energy revealing a small gap.

are given separately in the three lower panels of Figure 2. The states close to the Fermi level are dominated by Co 3d states and Os 5d states. The calculations converge to antiparallel alignment of the Co and Os spins, giving rise to a ferrimagnetic ground state. The Co 3d and Os 5d states are both spin and crystal-field split into approximately degenerate sets of t_{2g} and e_g states. DFT calculations show that minority spin Os t_{2g} states are partially filled with nominal occupancy of d^2, corresponding to an oxidation state of Os(VI). The Co^{2+} ion, which is found to be in a d^7 high-spin state, has its d states completely occupied in the majority spin channel, and partially filled t_{2g} states crossing the Fermi level (E_F) in the minority spin channel. Some splitting is observed within the Co e_g states, which is due to a larger distortion of the CoO_6 octahedra, which produces larger splitting of the d_{x2-y2} and d_{z2} orbitals in the DOS of Ca_2CoOsO_6 compared to that of the Ni e_g orbitals in Ca_2NiOsO_6.

DOI: 10.1021/acs.chemmater.6b00254
Chem. Mater. XXXX, XXX, XXX−XXX

Osmium, with spins aligned antiparallel to cobalt, has its t_{2g} states crossing the Fermi level in the minority spin channel. Thus, the bands close to E_F show an admixture of Os and Co t_{2g} character in the minority spin channel. The mixture is much more pronounced in the GGA calculations that do not involve U or SOC (see Supporting Information). The bare Os $t_{2g}-e_g$ splitting is about 4 eV, which gets renormalized by the bandwidth effect and spin-splitting effect. The Os e_g states are thus located far above the Fermi level and show minimal mixing with the Co 3d states. Introduction of spin−orbit coupling reconstructs the t_{2g} states, and splits them, opening up a very small gap in the minority spin channel making the system insulating, as shown in the inset to the upper panel of Figure 2. The size of the gap increases as the U values increase, but without accurate optical measurements of the gap it is difficult to use experimental data to set the values of U for Co and Os. We can however conclude that both correlations and spin−orbit effects are necessary to explain the insulating nature of Ca_2CoOsO_6. Similar behavior was previously found in the case of La_2CoMnO_6.[35]

The partial density of states plots for Ca_2NiOsO_6 are shown in Figure 3. Not surprisingly, they are qualitatively similar to Ca_2CoOsO_6, but now the minority spin Ni t_{2g} orbitals are completely below the Fermi energy, as expected for a d^8 Ni(II) ion. The Ni(II) contribution to the minority spin Os t_{2g} set of bands at the Fermi level is significantly smaller than it was in the case of Ca_2CoOsO_6, so much so that one might call it negligible. This may help explain why the conductivity of Ca_2NiOsO_6 is roughly 2 orders of magnitude smaller than that of Ca_2CoOsO_6. Here also both correlations and spin−orbit coupling must be used in the calculations to open a gap at E_F.

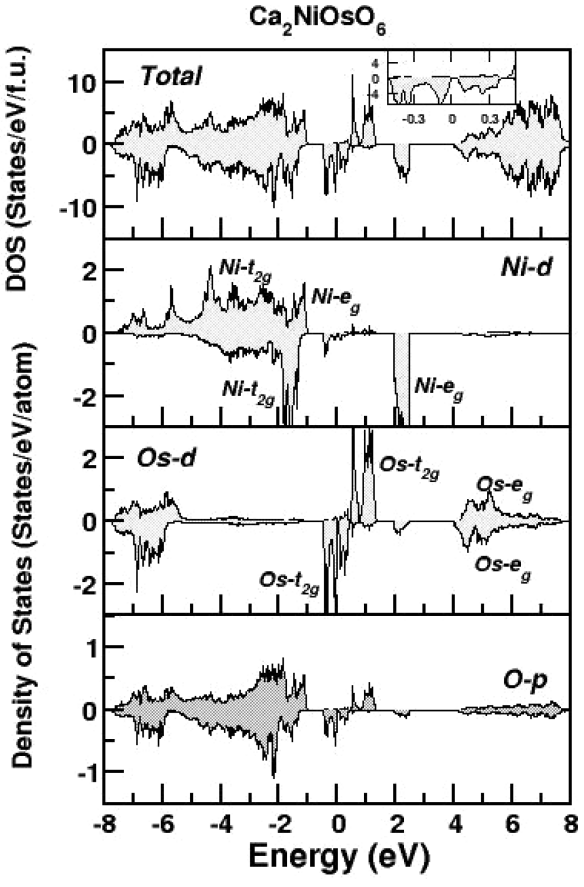

Figure 3. Spin dependent partial density of states plots for Ca_2NiOsO_6 as given by GGA+U+SOC calculations. The Fermi level is set to zero energy. The inset in the upper panel highlights the region near the Fermi energy revealing a small gap.

Having established that Ca_2CoOsO_6 and Ca_2NiOsO_6 contain localized electrons we next turn to the question of the magnitudes of the local moments. The local moments that come out of the DFT calculations are given in Table 1. In the simplest approximation one would expect the spin moments m_s to be equal to the number of unpaired electrons, namely, 3 for Co(II), 2 for Ni(II), and 2 for Os(VI). The calculated values of m_s are 10−20% smaller than the nominal values for Co(II) and Ni(II), and 50% smaller for Os(VI). This reduction is predominantly due to covalency with the surrounding oxide ions. Given its high oxidation state it is not surprising that the effect is largest for Os(VI).

Table 1. Spin (m_s), Orbital (m_l), and Total (m_{tot}) Magnetic Moments Calculated for Ca_2CoOsO_6 and Ca_2NiOsO_6

	Ca_2CoOsO_6	Ca_2NiOsO_6
m_s (Co/Ni)	+2.62 μ_B	+1.61 μ_B
m_l (Co/Ni)	+0.13 μ_B	+0.16 μ_B
m_{tot} (Co/Ni)	+2.75 μ_B	+1.76 μ_B
m_l/m_s (Co/Ni)	4.9%	9.8%
m_s (Os)	−1.05 μ_B	−0.98 μ_B
m_l (Os)	+0.34 μ_B	+0.34 μ_B
m_{tot} (Os)	−0.71 μ_B	−0.64 μ_B
m_l/m_s (Os)	−33%	−35%
m_{tot} (O)[b]	−0.04 μ_B	−0.04 μ_B
net magnetization[a]	1.57 μ_B/fu	0.61 μ_B/fu

[a]This is the sum of the magnetization over all atoms and interstitial space in the unit cell, divided by 2 to normalize the value to a single Ca_2MOsO_6 formula unit. [b]This is the average total magnetization per oxygen atom.

The orbital moments add to the spin moments for Co(II) and Ni(II), as expected for ions where the d-subshells are more than half-filled. The orbital and spin moments oppose each other for Os(VI), also in line with expectations. The magnitude of the orbital moment m_l for Os(VI) is calculated to be approximately one-third as large as the spin moment m_s.

The orbital moments for the 3d ions are calculated to be considerably smaller, roughly 5−10% of the spin moments. As discussed later these values seem to underestimate the experimentally observed size of the orbital moment for reasons which are not fully understood. There is a small but finite moment on oxygen that is parallel to the osmium moment, consistent with the highly covalent nature of the Os−O bonds.

The net magnetization values given in Table 1 were calculated by summing over the entire unit cell. When spin−orbit coupling is excluded from the calculations, the net magnetization is exactly 1 μ_B/formula unit (fu) for Ca_2CoOsO_6 where the Co(II) ion has one more unpaired electron than the Os(VI) ion, and 0 μ_B/fu for Ca_2NiOsO_6 where both ions have two unpaired electrons. As discussed above, spin−orbit coupling increases the Co(II)/Ni(II) moment and decreases the Os(VI) moment, both of which lead to an increase in the net magnetization. When SOC is included in the calculations, values of 1.57 μ_B/fu for Ca_2CoOsO_6 and 0.61 μ_B/fu for Ca_2NiOsO_6 are obtained.

Next we turn to experimental probes of the magnetism. The magnetic hysteresis loops for each compound are shown in

DOI: 10.1021/acs.chemmater.6b00254
Chem. Mater. XXXX, XXX, XXX−XXX

Figure 4. From these plots, saturation magnetization values are estimated to be 1.77 μ_B/fu for Ca_2CoOsO_6 and 0.48 μ_B/fu for

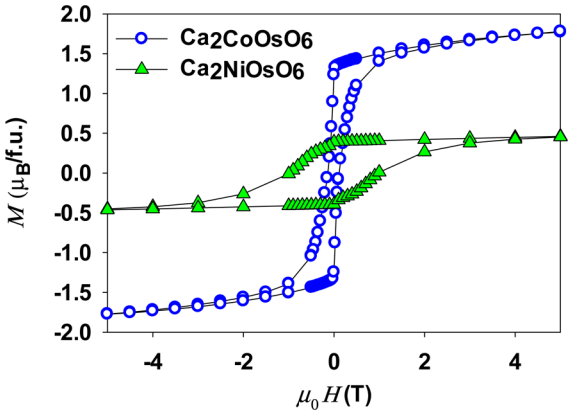

Figure 4. Field dependence of the magnetization of Ca_2CoOsO_6 and Ca_2NiOsO_6 as measured at 5 K.

Ca_2NiOsO_6. These values are in good agreement with previous reports[20,21] as well as with the calculated values. The measured coercivities are approximately 1.5 and 10 kOe for Ca_2CoOsO_6 and Ca_2NiOsO_6, respectively.

X-ray absorption spectroscopy measurements were made at the $L_{3,2}$ edges of the 3d transition metal ion at a temperature of 10 K and at the $L_{3,2}$ edges of Os at 5 K, as shown in Figure 5. Previous bond length analysis from neutron powder diffraction data has been used to assign the oxidation states as high-spin Co(II)/Os(VI) and Ni(II)/Os(VI) in agreement with the DFT results.[20,21] Nonetheless, the observed XAS L_3 and L_2 peak shapes and energies are consistent with the assignments of octahedrally coordinated high-spin Co(II) and Ni(II).[36] Oxidation state assignments for 5d cations are less straightforward to make from XAS data due to the closeness in L edge XAS peak shape and position for the different valencies,[37,38] but in the absence of large concentrations of defects (e.g., oxygen vacancies) the oxidation state assignments for osmium can be inferred to be Os(VI) from the stoichiometry and the oxidation state of the 3d ion.

XMCD sum rules[39] were applied to yield spin, orbital, and total moments for each transition metal as detailed in the Supporting Information. It is apparent from Figure 5 that the sign of the magnetic moment of each 3d transition metal is oppositely aligned to the Os moment, with the Os moment being oriented against the applied field during measurement. This observation, together with the absence of (purely) magnetic diffraction peaks in the neutron diffraction data, and the observed values of net magnetization, provides strong experimental support in favor of the ferrimagnetic model.

The absolute values of the moments can be obtained by normalizing the integrated XMCD data by the XAS data, as per the sum rules.[39] These values, which are given in the Supporting Information, are less accurate than the m_l/m_s ratios due to the need to accurately integrate the XAS data. The neglect of the magnetic dipole term in the spin sum rule is an additional source of error in the derived spin moment, particularly for Os. For example, in Sr_2FeOsO_6 it contributes a 20% correction to the Os spin moment.[15] Additionally, errors arising from core level mixing in 3d cations such as Ni(II) and Co(II) on the order of 10% should be taken into consideration.[40] Despite the rather large error bars on the

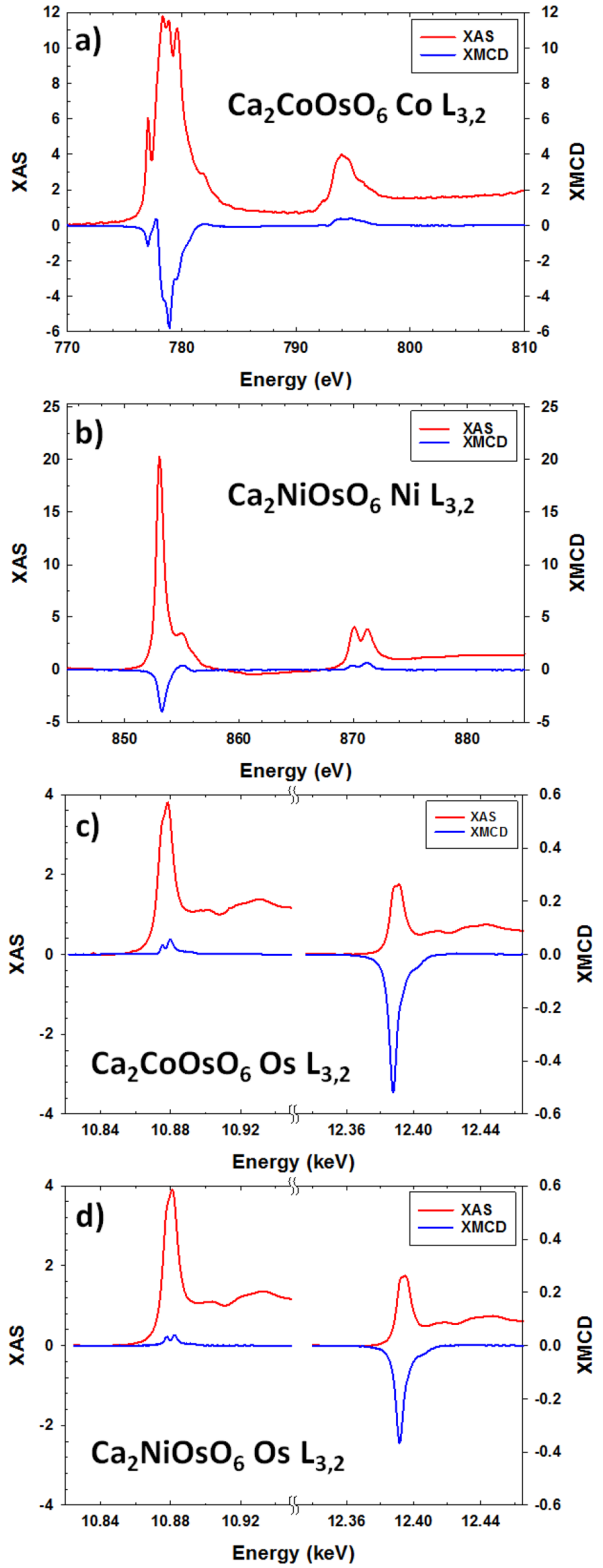

Figure 5. XAS and XMCD spectra of Ca_2CoOsO_6 (a, c) and Ca_2NiOsO_6 (b, d). The Co/Ni $L_{3,2}$ edges are shown in the top two panels, while the Os $L_{3,2}$ edges are shown in the bottom two panels. The data have been normalized to a 2:1 L_3 to L_2 step size. Arbitrary *y*-axis units are used for all spectra.

individual moments, there is no doubt that the Os(VI) ions have sizable local moments, at least as large if not larger than the computationally predicted values of 0.6−0.7 μ_B. Further-

DOI: 10.1021/acs.chemmater.6b00254
Chem. Mater. XXXX, XXX, XXX−XXX

more, the m_l/m_s ratios of 28% for Os(VI) in Ca_2CoOsO_6 and 29% in Ca_2NiOsO_6 are in good agreement with the calculated values. On the other hand, the m_l/m_s ratios of 29% for Ni(II) and 44% for Co(II) are much larger than those that are calculated. However, the presence of a significant orbital contribution is not unexpected for the high-spin d^7 configuration of the octahedrally coordinated Co(II) ion, where the orbital moment is generally not fully quenched.

One of the most striking features of osmate double perovskites is the sensitivity of the magnetic ground state to relatively subtle changes in M−O−Os bond angle. As mentioned in the Introduction, the tetragonal Sr_2MOsO_6 (M = Fe, Co, Ni, Cu) double perovskites are antiferromagnets,[13,14,17,21,22] while the monoclinic Ca_2MOsO_6 analogues are ferrimagnets.[14−16,20,21,23] This behavior implies that there are competing superexchange interactions, and some or all of those interactions are highly sensitive to distortions of the structure. While experimental probes like inelastic neutron scattering are the preferred method of assessing the sign and strength of the various coupling constants, the lack of large single crystals has hindered such efforts.

The M−O−Os bond angles in Ca_2CoOsO_6 and Ca_2NiOsO_6 are bent quite strongly away from the linear geometry of the aristotype cubic structure, to average values of 151° and 150°, respectively.[20,21] More importantly, all three crystallographically distinct bond angles are nearly equal (they fall within a 1.5° span in both compounds) so that the coupling between magnetic ions can safely be assumed to be isotropic, thereby simplifying the calculations.

The coupling constants derived from DFT total energy calculations of five different collinear spin configurations of Co/Ni and Os, and mapped onto an underlying spin model, are summarized in Table 2. Calculations were also carried out

Table 2. Computed Values of the Relevant Magnetic Coupling Constants for Ca_2MOsO_6 Perovskites[b]

exchange	description[a]	neighbors	M = Co	M = Ni
J_1	M−Os	6	−8.39	−10.82
J_2	M−M (NN)	12	−0.113	−0.075
J_3	Os−Os (NN)	12	+2.029	+2.716
J_4	M−M (NNN)	6	−0.368	−1.214
J_5	Os−Os (NNN)	6	+0.968	+0.294

[a]NN signifies nearest neighbors. NNN signifies next nearest neighbors. [b]Negative values of J signify antiferromagnetic coupling while positive values signify ferromagnetic coupling. The exchange pathways are illustrated in Figure 6.

considering nine different spin configurations assuming the in-plane and out-of-plane couplings to be different in choosing the spin configurations, but the difference between in-plane and out-of-plane couplings turned out to be small due to the more or less isotropic nature, mentioned above.

The magnetic interactions corresponding to each coupling constant are illustrated in Figure 6. The strongest interaction is the M−Os interaction J_1, which is not surprising since this is the shortest distance between magnetic ions. The negative sign, indicating antiferromagnetic coupling, is the observed ferrimagnetic ground state of these two compounds. We note here that, following the Goodenough−Kanamori prescription, the superexchange interaction between a transition metal ion with d^8 (or high-spin d^7) state and one with empty e_g orbitals (d^2 in the present case) should be ferromagnetic, as for example in

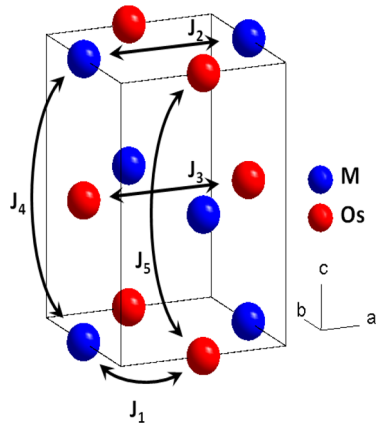

Figure 6. Relevant magnetic exchange interactions included in the computational modeling. Values for the coupling constants are given in Table 2.

La_2NiMnO_6[41] or La_2CoMnO_6.[35,42] This would have been the case if both metals were 3d transition metals ions where the t_{2g}−e_g crystal-field splitting is about 1−2 eV. However, because Os is a 5d transition metal, its t_{2g}−e_g crystal-field splitting is large, about 4 eV, and there is very poor energetic overlap with the e_g orbitals on Co/Ni. This in turn makes hybridization of Co/Ni e_g states with empty Os e_g states via oxygen negligible. We will return to this point in the Discussion section.

The relative magnitudes of the homonuclear M−M coupling constants J_2 and J_4 are consistent with the behavior of double perovskites containing a single late 3d transition metal ion (see Table S2 in the Supporting Information). The NNN coupling J_4 is larger than the NN coupling J_2, which in the absence of other interactions will stabilize the type II AFM structure seen for Ca_2CoWO_6 and Ca_2NiWO_6 (Figure S1 in Supporting Information).

An unexpected result is the observation that both Os−Os coupling constants, J_3 and J_5, are ferromagnetic. This is rather unexpected as there are no known examples of double perovskites where the only magnetic ion is a $5d^2$ (or $4d^2$) ion that is known to be a ferromagnet. Typically, Os(VI) ions in double perovskites like Ba_2CaOsO_6, Ca_2CaOsO_6, and Sr_2MgOsO_6 show antiferromagnetic behavior.[25−28] This is, however, a robust output of the calculation. We have checked this theoretical result considering variation in basis set and choice of U parameter over a reasonable range. It is worth noting that the J_5 pathway is experimentally confirmed to be ferromagnetic[17] in the antiferromagnet Sr_2CoOsO_6′ (or at least the moments connected by that pathway are aligned parallel). Intuitively, it thus seems like the Co(II) and Ni(II) ions play some role in changing the sign of the Os−Os exchange interactions. Presumably, the strong M−Os AFM interaction perturbs the Os−Os exchange, leading to FM exchange instead of the AFM exchange that is typically observed. While unexpected, the presence of ferromagnetic Os−Os coupling works cooperatively with the antiferromagnetic Os−M coupling to stabilize the ferrimagnetic state.

An indicative measure of the Curie temperature trend between the Co and Ni compounds may be obtained by considering the pseudosum, defined as $\sum J_k \cdot Z_k \cdot S_i \cdot S_j$, where the summation over k runs over the dominant magnetic interactions listed in Table 2. Z_k is the number of neighbors for the kth magnetic interaction, and S_i and S_j are the spin values of the magnetic sites at i and j defining the magnetic

DOI: 10.1021/acs.chemmater.6b00254
Chem. Mater. XXXX, XXX, XXX−XXX

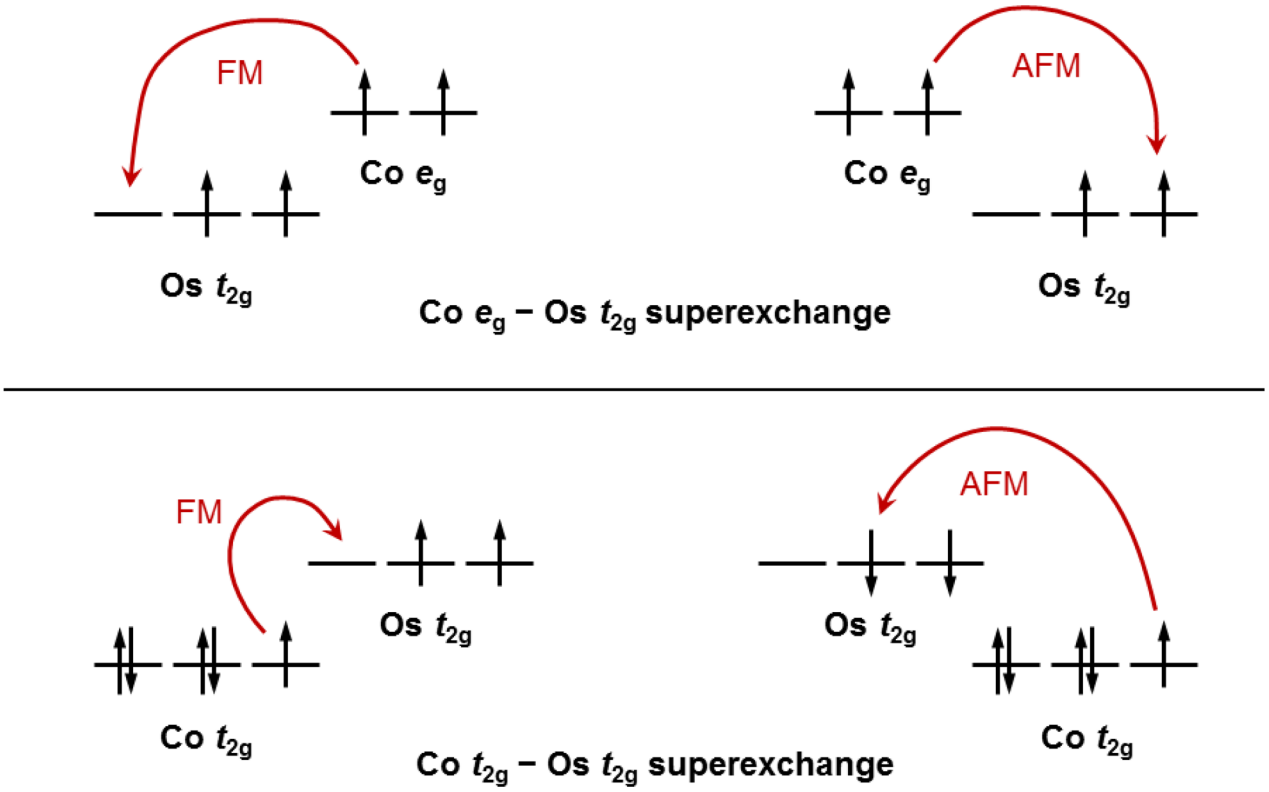

Figure 7. Potential superexchange interactions between the Os t_{2g} orbitals and the Co e_g orbitals (upper), and the Co t_{2g} orbitals (lower).

interactions. The spin values of Co(II), Ni(II), and Os(VI) are taken as 3/2, 1, and 1, respectively. Using the above parameters, we find the pseudosum to be negative, indicating dominance of antiferromagnetic interaction over the ferromagnetic interaction, thus stabilizing the observed ferrimagnetic solution. The ratio of the pseudosum of the calculated exchanges, together with spins for the Ni to Co compounds, is found to be 1.13, which is similar to the ratio of 175 K/145 K = 1.2 between the experimentally observed Curie temperatures of the two compounds.

DISCUSSION

Double perovskites like Sr_2FeMoO_6 and Sr_2CrWO_6 have been the focus of intense scrutiny due in part to their promise as half metallic conductors for use in spintronic applications.[43,44] Among the osmate double perovskites, Ca_2CoOsO_6 is one of the best candidates to be a half metallic conductor: the t_{2g} orbitals of both Os and Co are partially filled, there is little to no Co/Os antisite disorder, and the ferrimagnetic ordering is ideal for delocalization of the electrons in the Os 5d orbitals. While the room temperature conductivity of $\sim 10^3$ S cm^{-1} is appreciable, the temperature dependence of Ca_2CoOsO_6 rules out metallic conductivity. The DFT calculations show considerable hybridization between Os and Co t_{2g} orbitals at the Fermi level leading to an electronic structure that is tantalizingly close to a half metallic conductor. Nevertheless, the combined effects of electron correlations (modeled as $+U$) and spin−orbit coupling reduce that hybridization and open a small gap at E_F, which makes Ca_2CoOsO_6 an SOC assisted Mott insulator.

Ca_2NiOsO_6 is also insulating, but the conductivity drops by 2−3 orders of magnitude compared to that of Ca_2CoOsO_6. The decreased conductivity likely originates from the filling of the Ni t_{2g} bands, which prevents delocalization of the minority spin Os t_{2g} electrons via hybridization with Ni t_{2g} orbitals. This conclusion is supported by the electronic structure calculations. The partial DOS plots shown in Figure 3 reveal a much smaller contribution of the Ni 3d orbitals to the minority spin "Os t_{2g}" bands of Ca_2NiOsO_6 than the Co 3d orbital contribution to those same bands in Ca_2CoOsO_6.

The activated electrical transport of Ca_2CoOsO_6 and Ca_2NiOsO_6 can be compared with that of other ferrimagnetic double perovskites where the 5d ion has a d^2 configuration. For example Sr_2CrReO_6 and Ca_2FeReO_6 are also ferrimagnetic insulators.[45,46] It would appear that going from a double perovskite where the 4d/5d ion has a d^1 configuration (e.g., Sr_2FeMoO_6, Sr_2CrWO_6) to one where the 4d/5d ion has a d^2 configuration leads to increased electron correlations (i.e., a larger U) in the partially filled t_{2g} bands near E_F that act to localize the electrons. In that regard, it is pertinent to note that in our calculations a U term for Os must be included in order to reproduce the insulating behavior seen experimentally.

One of the main motivations behind this work was to assess the size of the local moment on the Os(VI) ion. While there is some spread in the exact value of the osmium moment, the magnetometry, XMCD measurements, and first-principles calculations all point to a finite moment on Os(VI). Both calculations and XMCD agree that the moment is reduced from its spin only value by approximately 30% due to spin−orbit coupling. The local moment on osmium is further reduced by covalency with oxygen that transfers some of the moment from osmium to the surrounding oxygen atoms.

Neutron diffraction is arguably the most straightforward technique for determining local moments. Unfortunately in double perovskites where Os(VI) is the only magnetic ion, researchers have not yet been able to measure the moment

DOI: 10.1021/acs.chemmater.6b00254
Chem. Mater. XXXX, XXX, XXX−XXX

using neutrons (Table S2 in Supporting Information).[23,25] However, in perovskites containing the d^3 Os(V) ion, such as Sr_2MOsO_6 (M = Sc, In, Y) and Ba_2YOsO_6, the neutron moment has consistently been found to be in the range 1.6−1.9 μ_B.[48−50] Going from the $5d^3$ configuration of Os(V) to the $5d^2$ configuration of Os(VI) should reduce the spin moment by a factor of 1/3. The increase in oxidation state should also increase covalency with oxygen, which will further reduce the Os moment seen by neutrons and XMCD. Finally, the SOC is expected to be much higher for the d^2 configuration further reducing the Os(VI) moment. When all of these factors are taken into account, the calculated Os(VI) moments of 0.6−0.7 μ_B given in Table 1 seem to be reasonable estimates. Moments of this size are just small enough to be below the detection limit of some neutron diffraction instruments, which could explain why the $5d^2$ Re(V) and Os(VI) moments in ferrimagnetic Ca_2CoOsO_6, Ca_2NiOsO_6, and Mn_2FeReO_6 have been difficult to observe.[20,21,47] Further support for this size of moment comes from the fact that Yan et al. found a moment of 0.7(1) μ_B for Os(VI) in Sr_2CoOsO_6.[18]

The Os(VI) moments estimated from the XMCD data using the sum rules are somewhat larger, 0.86 μ_B in Ca_2NiOsO_6 and 1.4 μ_B in Ca_2CoOsO_6 (Table S3 in Supporting Information). It appears that the experimental uncertainties associated with estimating the absolute value of the moment using the sum rules lead to an overestimation of the Os(VI) moment, particularly for Ca_2CoOsO_6.

Finally, we turn to the question of the sign and relative magnitude of the various superexchange coupling interactions in these compounds. Here we focus on two key points: the failure of the Goodenough−Kanamori rules[11,12] to predict the sign of the Os−Co/Ni superexchange coupling, and the unexpected observation of ferromagnetic Os−Os coupling.

Filling of the e_g orbitals is the basis for the G-K rules. In these two compounds the combination of half-filled e_g orbitals on Co(II)/Ni(II) and empty e_g orbitals on Os(VI) should lead to ferromagnetic coupling, a prediction that is in disagreement with both calculations and experimental observations. However, as pointed out above, being a 5d transition metal, the t_{2g}−e_g crystal-field splitting in Os is large, thus driving the e_g states out of the picture.

If Os e_g−Co/Ni e_g interactions are not playing an important role, what types of orbital interactions are leading to the strong antiferromagnetic coupling of the ions? In Ca_2NiOsO_6 the Ni t_{2g} orbitals are completely filled, which rules out Os t_{2g}−Ni t_{2g} interactions. The only realistic superexchange interaction remaining is between the half-filled e_g orbitals on Ni(II) and the partially filled t_{2g} orbitals on Os(VI). While these two sets of orbitals are orthogonal in the cubic double perovskite structure, that is not the case in the monoclinic structures that Ca_2NiOsO_6 and Ca_2CoOsO_6 adopt.

Using simple electron exchange pathways we can rationalize the sign of the net magnetic interaction between Co(II)/Ni(II) and Os(VI). There is an interplay of ferromagnetic and antiferromagnetic contributions from different channels (see upper panel of Figure 7). The antiferromagnetic contribution is due to virtual exchange between the half-filled Co(II)/Ni(II) e_g orbitals and the two half-filled Os t_{2g} orbitals, while the ferromagnetic contribution is due to virtual exchange between the half-filled Co(II)/Ni(II) e_g orbitals and the single empty Os t_{2g} orbital. Because there are two half-filled Os t_{2g} orbitals and only one empty Os t_{2g} orbital, the number of antiferromagnetic interactions is double the number of ferromagnetic interactions. Thus, the Os−O−Ni/Co coupling is antiferromagnetic, in spite of the Hund's energy gain that accompanies the ferromagnetic exchange pathway.

Two additional interaction channels open up in Ca_2CoOsO_6: an antiferromagnetic coupling between the Co(II) t_{2g} orbital that contains only one electron and the Os t_{2g} orbitals that are half-filled, and ferromagnetic coupling between the same Co(II) t_{2g} orbital and the empty Os t_{2g} orbital. These are depicted in the lower panel of Figure 7. Once again the number of antiferromagnetic channels is greater than that of the ferromagnetic channels, thus favoring a net antiferromagnetic Co−Os interaction.

We are now in a position to understand why the magnetic ground states of $Sr_{2-x}Ca_xMOsO_6$ (M = Co, Ni) double perovskites are so sensitive to chemical and external pressure. If the antiferromagnetic coupling of Os−O−M involves virtual hopping between e_g and t_{2g} orbitals as suggested here, the J_1 term should become smaller as the bonds become more linear, as is the case in Sr_2CoOsO_6 and Sr_2NiOsO_6. Since J_1 is the primary driving force behind formation of the ferrimagnetic state, it is not surprising to see ferrimagnetism give way to antiferromagnetism as the bonds become more linear. Not only will the strength of J_1 decrease, the longer range antiferromagnetic Co−Co and Ni−Ni exchange interactions, J_4 in Figure 6, are likely to become stronger as the Os−O−M bond angle approaches 180°.

The ferromagnetic nature of Os−Os interaction, as revealed in our study, is interesting and demands attention. Investigation of the effective Os t_{2g} Wannier function (Figure S4 in the Supporting Information) shows little weight at the Co/Ni site, thus hinting that the 3d cation makes little contribution to the exchange path between Os atoms. Taken at face value this result suggests that the Os−O−O−Os exchange pathway is the dominant exchange pathway. Therefore, the dihedral angle involving Os−O−O−Os atoms should be important, especially for the NN Os−Os interaction, for which the value of the exchange interaction is found to be substantial (see Table 2). This dihedral angle is small in the studied compounds (∼30−35°). This angle may be compared with that in the antiferromagnet Ca_2CaOsO_6 in which it is 60.4°.[25] Further studies of the effects of the Os−O−O−Os dihedral angle on Os−Os superexchange coupling are needed to confirm or refute this preliminary hypothesis. There is a precedent for a crossover from antiferromagnetic to ferromagnetic coupling in a double perovskite driven by a change in the octahedral tilting. Sr_2CrSbO_6 is antiferromagnetic with T_N = 12 K, while the isoelectronic Ca_2CrSbO_6, which exhibits a larger octahedral tilting distortion, is ferromagnetic with T_C = 16 K.[51,52]

CONCLUSIONS

The magnetic moments and superexchange coupling in the ferrimagnetic double perovskites Ca_2CoOsO_6 and Ca_2NiOsO_6 have been studied. Calculations suggest the local moment on the d^2 Os(VI) ion is 0.6−0.7 μ_B. The moment is reduced by approximately 50% by covalency with oxygen and by another 30% by spin−orbit coupling. XMCD measurements confirm the degree of spin−orbit coupling obtained in the calculations. The ferrimagnetism is driven by antiferromagnetic Os−O−Co/Ni superexchange coupling involving half-filled e_g orbitals of the 3d ion and partially filled t_{2g} orbitals of the 5d ion. The strength of this superexchange coupling decreases as the Os−O−Co/Ni bond angle approaches a linear configuration where intersite t_{2g}−e_g coupling is symmetry forbidden. Finally, the combined

DOI: 10.1021/acs.chemmater.6b00254
Chem. Mater. XXXX, XXX, XXX−XXX

effects of spin−orbit coupling and electron correlations lead to a localized electron insulator instead of a half metallic conductor.

■ ASSOCIATED CONTENT

Supporting Information

The Supporting Information is available free of charge on the ACS Publications website at DOI: 10.1021/acs.chemmater.6b00254.

Table of theoretical weak- and strong-field free ion moments of relevant cations; table of the magnetic properties of double perovskites containing a single similar magnetic cation together with an illustration of important exchange pathways for such compounds, GGA, GGA+U, and GGA+U+SOC DOS as well as PDOS plots for Ca_2CoOsO_6 and Ca_2NiOsO_6; a table of XMCD sum rule analysis results; and a Wannier function figure for Ca_2CoOsO_6 (PDF)

■ AUTHOR INFORMATION

Corresponding Authors

*E-mail: t.sahadasgupta@gmail.com.
*E-mail: woodward@chemistry.ohio-state.edu.

Notes

The authors declare no competing financial interest.

■ ACKNOWLEDGMENTS

Support for this research was provided by the Center for Emergent Materials, an NSF Materials Research Science and Engineering Center (DMR-1420451). Use of the Advanced Photon Source was supported by the U.S. Department of Energy, Office of Science, Office of Basic Energy Sciences, under Contract DE-AC02-06CH11357. K.S and T.S.D. acknowledge the support from Department of Science and Technology, India, through Thematic Unit of Excellence on Computational Materials Science. The authors would like to gratefully acknowledge the assistance of Yongseong Choi in the collection of Os XAS/XMCD data on beamline 4-ID-D.

■ REFERENCES

(1) Cao, G.; Bolivar, J.; McCall, S.; Crow, J. E.; Guertin, R. P. Weak Ferromagnetism, Metal-to-Nonmetal Transition, and Negative Differential Resistivity in Single-Crystal Sr_2IrO_4. *Phys. Rev. B: Condens. Matter Mater. Phys.* **1998**, *57*, R11039.

(2) Kim, B. J.; Ohsumi, H.; Komesu, T.; Sakai, S.; Morita, T.; Takagi, H.; Arima, T. Phase-Sensitive Observation of a Spin-Orbital Mott State in Sr_2IrO_4. *Science* **2009**, *323*, 1329−1332.

(3) Perry, R. S.; Baumberger, F.; Balicas, L.; Kikugawa, N.; Ingle, N. J. C.; Rost, A.; Mercure, J. F.; Maeno, Y.; Shen, Z. X.; Mackenzie, A. P. Sr_2RhO_4: A New Clean Correlated Electron Metal. *New J. Phys.* **2006**, *8*, 175.

(4) Morrow, R.; Susner, M. A.; Sumption, M. D.; Woodward, P. M. Magnetic Structure of the Quasi-One-Dimensional La_3OsO_7 as Determined by Neutron Powder Diffraction. *Phys. Rev. B: Condens. Matter Mater. Phys.* **2015**, *92*, 134402.

(5) Lam, R.; Wiss, F.; Greedan, J. E. Magnetic Properties of the Fluorite-Related La_3MO_7 Phases, *M* = Ru and Os: Local Moment Magnetism, Short- and Long-Range Order in 4d and 5d Transition Metal Oxides. *J. Solid State Chem.* **2002**, *167*, 182−187.

(6) Khalifah, P.; Erwin, R. W.; Lynn, J. W.; Huang, Q.; Batlogg, B.; Cava, R. J. Magnetic and Electronic Characterization of Quasi-One-Dimensional La_3RuO_7. *Phys. Rev. B: Condens. Matter Mater. Phys.* **1999**, *60*, 9573.

(7) Singh, Y.; Manni, S.; Reuther, J.; Berlijn, T.; Thomale, R.; Ku, W.; Trebst, S.; Gegenwart, P. Relevance of the Heisenberg-Kitaev Model for the Honeycomb Latticec Iridates A_2IrO_3. *Phys. Rev. Lett.* **2012**, *108*, 127203.

(8) Chaloupka, J.; Jackeli, G.; Khaliullin, G. Kitaev-Heisenberg Model on a Honeycomb Lattice: Possible Exotic Phases in Iridium Oxides A_2IrO_3. *Phys. Rev. Lett.* **2010**, *105*, 027204.

(9) Chun, S. H.; Kim, J. W.; Kim, J.; Zheng, H.; Stoumpos, C. C.; Malliakas, C. D.; Mitchell, J. F.; Mehlawat, K.; Singh, Y.; Choi, Y.; Gog, T.; Al-Zein, A.; Sala, M. M.; Krisch, M.; Chaloupka, J.; Jackeli, G.; Khaliullin, G.; Kim, B. J. Direct Evidence for Dominant Bond-Directional Interactions in a Honeycomb Lattice Iridate Na_2IrO_3. *Nat. Phys.* **2015**, *11*, 462−466.

(10) Witczak-Krempa, W.; Chen, G.; Kim, Y. B.; Balents, L. Correlated Quantum Phenomena in the Strong Spin-Orbit Regime. *Annu. Rev. Condens. Matter Phys.* **2014**, *5*, 57−82.

(11) Goodenough, J. B. Theory of the Role of Covalence in the Perovskite-Type Manganites [La, M(II)]MnO_3. *Phys. Rev.* **1955**, *100*, 564−573.

(12) Kanamori, J. Superexchange Interaction and Symmetry Properties of Electron Orbitals. *J. Phys. Chem. Solids* **1959**, *10*, 87−98.

(13) Paul, A. K.; Reehuis, M.; Ksenofontov, V.; Yan, B.; Hoser, A.; Tobbens, D. M.; Abdala, P. M.; Jansen, M.; Felser, C.; Adler, P. Lattice Instability and Competing Spin Strucutres in the Double Perovskite Insulator Sr_2FeOsO_6. *Phys. Rev. Lett.* **2013**, *111*, 167205.

(14) Morrow, R.; Freeland, J. W.; Woodward, P. M. Probing the Links between Structure and Magnetism in $Sr_{2-x}Ca_xFeOsO_6$ Double Perovskites. *Inorg. Chem.* **2014**, *53*, 7983−7992.

(15) Veiga, L. S. I.; Fabbris, G.; van Veenendaal, M.; Souza-NEto, N. M.; Feng, H. L.; Yamaura, K.; Haskel, D. Fragility of ferromagnetic double exchange interactions and pressure tuning of magnetism in 3*d*−5*d* double perovskite Sr_2FeOsO_6. *Phys. Rev. B: Condens. Matter Mater. Phys.* **2015**, *91*, 235135.

(16) Feng, H. L.; Arai, M.; Matsushita, Y.; Tsujimoto, Y.; Guo, Y.; Sathish, C. I.; Wang, X.; Yuan, Y.; Tanaka, M.; Yamaura, K. High-Temperature Ferrimagnetism Driven by Lattice Distortion in Doube Perovskite Ca_2FeOsO_6. *J. Am. Chem. Soc.* **2014**, *136*, 3326−3329.

(17) Morrow, R.; Mishra, R.; Restrepo, O. R.; Ball, M. R.; Windl, W.; Wurmehl, S.; Stockert, U.; Büchner, B.; Woodward, P. M. Independent Ordering of Two Interpenetrating Magnetic Sublattices in the Double Perovskite Sr_2CoOsO_6. *J. Am. Chem. Soc.* **2013**, *135*, 18824−18830.

(18) Yan, B.; Paul, A. K.; Kanungo, S.; Reehuis, M.; Hoser, A.; Többens, D. M.; Schnelle, W.; Williams, R. C.; Lancaster, T.; Xiao, F.; Möller, J. S.; Blundell, S. J.; Hayes, W.; Felser, C.; Jansen, M. Lattice-Site-Specific Spin Dynamics in Double Perovskite Sr_2CoOsO_6. *Phys. Rev. Lett.* **2014**, *112*, 147202.

(19) Paul, A. K.; Reehuis, M.; Felser, C.; Abdala, P. M.; Jansen, M. Synthesis, Crystal Structure, and Properties of the Ordered Double Perovskite Sr_2CoOsO_6. *Z. Anorg. Allg. Chem.* **2013**, *639*, 2421−2425.

(20) Morrow, R.; Yan, J.-Q.; McGuire, M. A.; Freeland, J. W.; Haskel, D.; Woodward, P. M. Effects of Chemical Pressure on the Magnetic Ground States of the Osmate Double Perovskites $SrCaCoOsO_6$ and Ca_2CoOsO_6. *Phys. Rev. B: Condens. Matter Mater. Phys.* **2015**, *92*, 094435.

(21) Macquart, R.; Kim, S. J.; Gemmill, W. R.; Stalick, J. K.; Lee, Y.; Vogt, T.; Zur Loye, H. C. Synthesis, Structure, and Magnetic Properties of Sr_2NiOsO_6 and Ca_2NiOsO_6: Two New Osmium-Containing Double Perovskites. *Inorg. Chem.* **2005**, *44*, 9676−9683.

(22) Lufaso, M. W.; Gemmill, W. R.; Mugavero, S. J.; Kim, S. J.; Lee, Y.; Vogt, T.; zur Loye, H. C. Synthesis, Structure, Magnetic Properties, and Structural Distortion under High Pressure of a New Osmate, Sr_2CuOsO_6. *J. Solid State Chem.* **2008**, *181*, 623−627.

(23) Morrow, R. Ph.D. Dissertation. *Competing Superexchange Interactions in Double Perovskite Osmates*. Ohio State University, 2015.

(24) Yamaura, K. Short Review of High-Pressure Crystal growth and Magnetic and Electrical Properties of Solid-State Osmium Oxides. *J. Solid State Chem.* **2016**, *236*, 45−54.

DOI: 10.1021/acs.chemmater.6b00254
Chem. Mater. XXXX, XXX, XXX−XXX

(25) Thompson, C. M.; Carlo, J. P.; Flacau, R.; Aharen, T.; Leahy, I. A.; Pollichemi, J. R.; Munsie, T. J. S.; Medina, T.; Luke, G. M.; Munevar, J.; Cheung, S.; Goko, T.; Uemura, Y. J.; Greedan, J. E. Long-Range Magnetic Order in the $5d^2$ Double Perovskite Ba_2CaOsO_6: Comparison with Spin-Disordered Ba_2YReO_6. *J. Phys.: Condens. Matter* **2014**, *26*, 306003.
(26) Feng, H. L.; Shi, Y.; Guo, Y.; Li, J.; Sato, A.; Sun, Y.; Wang, X.; Yu, S.; Sathish, C. I.; Yamaura, K. High-Pressure Crystal Growth and Electromagnetic Properties of 5d Double-Perovskite Ca_3OsO_6. *J. Solid State Chem.* **2013**, *201*, 186−190.
(27) Sarapulova, A.; Adler, P.; Schnelle, W.; Mikhailova, D.; Felser, C.; Tjeng, L. H.; Jansen, M. Sr_2MgOsO_6: A Frustrated Os^{6+} ($5d^2$) Double Perovskite with Strong Antiferromagnetic Interactions. *Z. Anorg. Allg. Chem.* **2015**, *641*, 769−771.
(28) Yuan, Y.; Feng, H. L.; Ghimire, M. P.; Matsushita, Y.; Tsujimoto, Y.; He, J.; Tanaka, M.; Katsuya, Y.; Yamaura, K. High-Pressure Synthesis, Crystal Structures, and Magnetic Properties of 5d Double-Perovskite Oxides Ca_2MgOsO_6 and Sr_2MgOsO_6. *Inorg. Chem.* **2015**, *54*, 3422−3431.
(29) Blaha, P.; Schwarz, K.; Madsen, G. K. H.; Kvasnicka, D.; Luitz, J. *WIEN2k, An Augmented Plane WaVe + Local Orbitals Program for Calculating Crystal Properties*; Technische Universität Wien: Wien, Austria, 2001.
(30) Perdew, J. P.; Burke, K.; Ernzerhof, M. Generalized Gradient Approximation Made Simple. *Phys. Rev. Lett.* **1996**, *77*, 3865.
(31) Dudarev, S. L.; Botton, G. A.; Savrasov, S. Y.; Humphreys, C. J.; Sutton, A. P. Electron-Energy Loss Spectra and the Structural Stability of Nickel Oxide: An LSDA + U Study. *Phys. Rev. B: Condens. Matter Mater. Phys.* **1998**, *57*, 1505.
(32) Andersen, O. K.; Jepsen, O. Linear Methods in Band Theory. *Phys. Rev. B* **1975**, *12*, 3060.
(33) Andersen, O. K.; Saha-Dasgupta, T. Muffin-Tin Orbitals of Arbitrary Order. *Phys. Rev. B: Condens. Matter Mater. Phys.* **2000**, *62*, R16219.
(34) Mott, N. F. Conduction in Non-Crystalline Solids. *Philos. Mag.* **1969**, *19*, 835−852.
(35) Baidya, S.; Saha-dasgupta, T. Electronic Structure and Phonons in La_2CoMnO_6: A Ferromagnetic Insulator Driven by Coulomb-Assisted Spin-Orbit Coupling. *Phys. Rev. B: Condens. Matter Mater. Phys.* **2011**, *84*, 035131.
(36) Montoro, L. A.; Abbate, M.; Almeida, E. C.; Rosolen, J. M. Electronic Structure of the Transition Metal Ions in $LiCoO_2$, $LiNiO_2$, and $LiCo_{0.5}Ni_{0.5}O_2$. *Chem. Phys. Lett.* **1999**, *309*, 14−18.
(37) Choy, J. H.; Kim, D. K.; Kim, J. Y. Study of the Electronic Structural Variation of Transition Metal Oxides by X-ray Absorption Spectroscopy. *Solid State Ionics* **1998**, *108*, 159−163.
(38) Laguna-Marco, M. A.; Kayser, P.; Alonso, J. A.; Martinez-Lope, M. J.; van Veenendaal, M.; Choi, Y.; Haskel, D. Electronic structure, local magnetism, and spin-orbit effects of Ir(IV)-, Ir(V)-, and Ir(VI)-based compounds. *Phys. Rev. B: Condens. Matter Mater. Phys.* **2015**, *91*, 214433.
(39) Chen, C. T.; Idzerda, Y. U.; Lin, H.-J.; Smith, N. V.; Meigs, G.; Chaban, E.; Ho, G. H.; Pellegrin, E.; Sette, F. Experimental Confirmation of the X-ray Magnetic Circular Dichroism Sum Rules for Iron and Cobalt. *Phys. Rev. Lett.* **1995**, *75*, 152−155.
(40) Teramura, Y.; Tanaka, A.; Jo, T. Effect of Coulomb Interaction on the X-Ray Magnetic Circular Dichroism Spin Sum Rule in 3*d* Transition Elements. *J. Phys. Soc. Jpn.* **1996**, *65*, 1053.
(41) Haskel, D.; Fabbris, G.; Souza-Neto, N. M.; van Veenendaal, M.; Shen, G.; Smith, A. E.; Subramanian, M. A. Stability of the ferromagnetic ground state of La_2MnNiO_6 against large compressive stress. *Phys. Rev. B: Condens. Matter Mater. Phys.* **2011**, *84*, 100403.
(42) Das, H.; Waghmare, U. V.; Saha-Dasgupta, T.; Sarma, D. D. Theoretical Evidence and Chemical Origin of the Magnetism-Dependent Electrostructural Coupling in La_2NiMnO_6. *Phys. Rev. B: Condens. Matter Mater. Phys.* **2009**, *79*, 144403.
(43) Kobayashi, K.-I.; Kimura, T.; Sawada, H.; Terakura, K.; Tokura, Y. Room-Temperature Magnetoresistance in an Oxide Material with an Ordered Double-Perovskite Structure. *Nature* **1998**, *395*, 677−680.
(44) Philipp, J. B.; Reisinger, D.; Schonecke, M.; Marx, A.; Erb, A.; Alff, L.; Gross, R.; Klein, J. Spin-Dependent Transport in the Double-Perovskite Sr_2CrWO_6. *Appl. Phys. Lett.* **2001**, *79*, 3654.
(45) Kato, H.; Okuda, T.; Okimoto, Y.; Tomioka, Y.; Oikawa, K.; Kamiyama, T.; Tokura, Y. Structural and Electronic Properties of the Ordered Double Perovskites A_2MReO_6 (A = Sr, Ca; M = Mg, Sc, Cr, Mn, Fe, Co, Ni, Zn). *Phys. Rev. B: Condens. Matter Mater. Phys.* **2004**, *69*, 184412.
(46) Hauser, A. J.; Soliz, J. R.; Dixit, M.; Williams, R. E. A.; Susner, M. A.; Peters, B.; Mier, L. M.; Gustafson, T. L.; Sumption, M. D.; Fraser, H. L.; Woodward, P. M.; Yang, F. Y. Fully Ordered Sr_2CrReO_6 Epitaxial Films: A High-Temperature Ferrimagnetic Semiconductor. *Phys. Rev. B: Condens. Matter Mater. Phys.* **2012**, *85*, 161201.
(47) Li, M. R.; Retuerto, M.; Deng, Z.; Stephens, P. W.; Croft, M.; Huang, Q.; Wu, H.; Deng, X.; Kotliar, G.; Sánchez-Benítez, J.; Hadermann, J.; et al. Giant Magnetoresistance in the Half-Metallic Double-Perovskite Ferrimagnet Mn_2FeReO_6. *Angew. Chem.* **2015**, *127*, 12237−12241.
(48) Kermarrec, E.; Marjerrison, C. A.; Thompson, C. M.; Maharaj, D. D.; Levin, K.; Kroeker, S.; Granroth, G. E.; Flacau, R.; Yamani, Z.; Greedan, J. E.; Gaulin, B. D. Frustrated fcc antiferromagnet Ba_2YOsO_6: Structural characterization, magnetic properties, and neutron scattering. *Phys. Rev. B: Condens. Matter Mater. Phys.* **2015**, *91*, 075133.
(49) Taylor, A. E.; Morrow, R.; Singh, D. J.; Calder, S.; Lumsden, M. D.; Woodward, P. M.; Christianson, A. D. Magnetic order and electronic structure of the $5d^3$ double perovskite Sr_2ScOsO_6. *Phys. Rev. B: Condens. Matter Mater. Phys.* **2015**, *91*, R100406.
(50) Paul, A. K.; Sarapulova, A.; Adler, P.; Reehuis, M.; Kanungo, S.; Mikhailova, D.; Schnelle, W.; Hu, Z.; Kuo, C.; Siruguri, V.; Rayaprol, S.; Soo, Y.; Yan, B.; Felser, C.; Hao Tjeng, L.; Jansen, M. Magnetically Frustrated Double Perovskites: Synthesis, Structural Properties, and Magnetic Order of Sr_2BOsO_6 (B = Y, In, Sc). *Z. Anorg. Allg. Chem.* **2015**, *641*, 197−205.
(51) Retuerto, M.; Garcia-Hernandez, M.; Martinez-Lope, M. J.; Fernandez-Diaz, M. T.; Attfield, J. P.; Alonso, J. A. Switching from ferro- to antiferromagnetism in A2CrSbO6 (A = Ca, Sr) double perovskites: a neutron diffraction study. *J. Mater. Chem.* **2007**, *17*, 3555−3561.
(52) Baidya, S.; Saha-Dasgupta, T. Effect of A cation on magnetic properties of double perovskite compounds: From ferromagnetic Ca_2CrSbO_6 to antiferromagnetic Sr_2CrSbO_6. *Phys. Rev. B: Condens. Matter Mater. Phys.* **2012**, *86*, 024440.

DOI: 10.1021/acs.chemmater.6b00254
Chem. Mater. XXXX, XXX, XXX−XXX